DOI: 10.1002/chem.200800125

Heterometallic [Mn_5-Ln_4] Single-Molecule Magnets with High Anisotropy Barriers

Valeriu Mereacre,[a] Ayuk M. Ako,[a] Rodolphe Clérac,*[b] Wolfgang Wernsdorfer,[c] Ian J. Hewitt,[a] Christopher E. Anson,[a] and Annie K. Powell*[a]

Abstract: The reaction of $[Mn_6O_2(Piv)_{10}(4\text{-Me-py})_{2.5}(PivH)_{1.5}]$ (**1**) (py: pyridine, Piv: pivilate) with *N*-methyldiethanolamine ($mdeaH_2$) and $Ln(NO_3)_3{\cdot}6H_2O$ in MeCN leads to a series of nonanuclear compounds $[Mn_5Ln_4(O)_6(mdea)_2(mdeaH)_2(Piv)_6(NO_3)_4(H_2O)_2]{\cdot}2MeCN$ ($Ln = Tb^{III}$ (**2**), Dy^{III} (**3**), Ho^{III} (**4**), Y^{III} (**5**)). Single-crystal X-ray diffraction shows that compounds **2**–**5** are isostructural, with the central core composed of two distorted $\{Mn^{IV}Mn^{III}Ln_2O_4\}$ cubanes sharing a Mn^{IV} vertex, representing a new heterometallic 3d–4f motif for this class of ligand. The four new compounds display single-molecule magnet (SMM) behaviour, which is modulated by the lanthanide ion used. Moreover, the values found for Δ_{eff} and τ_o for **3** of 38.6 K and 3.0×10^{-9} s respectively reveal that the complex **3** exhibits the highest energy barrier recorded so far for 3d–4f SMMs. The slow relaxation of the magnetisation for **3** was confirmed by μ-SQUID measurements on an oriented single crystal and the observation of *M* versus *H* hysteresis loops below 1.9 K.

Keywords: cluster compounds · lanthanides · magnetic properties · manganese · single-molecule magnets

Introduction

In spite of intense efforts on the part of the synthetic community, rather little progress has been made on improving on the parameters found for the very first example of a molecule shown to have single-molecule magnet (SMM) properties,[1] namely the $Mn_{12}OAc$ molecule first isolated by Lis.[2] This discovery of SMM behaviour prompted the synthesis and characterisation of huge numbers of interesting and beautiful 3d magnetically coupled metal aggregates in the quest for SMMs with high blocking temperatures and thus slow relaxation time of the magnetisation. This characteristic time follows an Arrhenius law that is governed by the magnitude of the barrier to reorientation of the spin, Δ_{eff}, and the pre-exponential factor, τ_o. Physicists have studied and explained these type of molecular systems over the years and established the key role played by the magnetic anisotropy and the high-spin ground state of a given complex to exhibit SMM properties.[3] Based on these investigations, synthetic chemists have explored new routes to multinuclear complexes, mostly incorporating the Mn^{III} ion,[4–7] which have high- (and isolated) spin ground states along with uniaxial anisotropy of the magnetisation. Until recently[8] no example could be found surpassing all the characteristics of the original Mn_{12} systems. In this recent breakthrough[8] the structural distortion of the core of a manganese hexanuclear compound switched the magnetic exchange interactions among metal centres from antiferromagnetic to ferromagnetic resulting in a molecule with an effective energy barrier Δ_{eff} of 86.4 K and $\tau_o = 2\times10^{-7}$ s.

Attention also turned towards introducing metal ions with different open-shell configurations. A seemingly evident early goal of research into molecular-based magnetism was to utilise the high spin available by incorporating 4f ions into 3d systems.[9] Earlier efforts mostly concentrated on

[a] Dr. V. Mereacre, Dr. A. M. Ako, Dr. I. J. Hewitt, Dr. C. E. Anson, Prof. A. K. Powell
Institut für Anorganische Chemie der Universität Karlsruhe
Engesserstr. Geb. 30.45, 76128 Karlsruhe (Germany)
Fax: (+49) 721-608-8142
E-mail: powell@aoc.uni-karlsruhe.de

[b] Dr. R. Clérac
Université Bordeaux 1, CNRS
Centre de Recherche Paul Pascal–UPR8641
115 av. du Dr. Albert Schweitzer, 33600 Pessac (France)
Fax: (+33) 556-84-56-00
E-mail: clerac@crpp-bordeaux.cnrs.fr

[c] Prof. W. Wernsdorfer
Institut Néel CNRS, BP 166
25 av. des Martyrs, 38042 Grenoble (France)

Supporting information for this article is available on the WWW under http://www.chemeurj.org/ or from the author.

Cu/Gd systems, which are inherently ferromagnetically coupled and produce high-spin ground states, but show negligible anisotropy.[10] Recently, a new approach has been to combine 3d and 4f metal ions that exhibit high-spin and/or single-ion anisotropy. For example, Cu_6Dy_3 or Co_2Gd compounds were recently reported with Δ_{eff} around 25 to 28 K and τ_o around $1–2\times10^{-7}$ s.[11] Similarly, the combination of manganese and lanthanides should provide an attractive way forward in developing the SMM properties of such systems. For example, we reported on a bell-shaped SMM $[Mn_{11}Gd_2]$[12] complex synthesised using the pre-formed hexanuclear $[Mn_6O_2(Piv)_{10}(4\text{-Me-py})_{2.5}(PivH)_{1.5}]$ (py: pyridine, Piv: pivalate) complex (**1**). Given that we had previously demonstrated how the use of N-substituted diethanolamine and related ligands in the synthesis of Mn_4 SMMs allowed us to obtain enhanced barrier heights to the reorientation of the spin relative to previous examples in the literature,[13] we decided to combine these approaches. Our aim was to discover if using the preformed complex **1** along with lanthanide salts and N-substituted diethanolamine in a similar synthetic procedure would give a route to producing 3d–4f SMMs with enhanced properties over the currently known examples.[11,12,14]

Results and Discussion

Synthesis and crystal structures: The reaction of **1** with *N*-methyldiethanolamine ($mdeaH_2$) and $Ln(NO_3)_3{\cdot}6H_2O$ in 1:11:6 molar ratio in MeCN gave a brown solution from which dark-brown crystals of $[Mn_3Ln_4(O)_6(mdea)_2(mdeaH)_2(Piv)_6(NO_3)_4(H_2O)_2]{\cdot}2MeCN$ (Ln = Tb^{III} (**2**), Dy^{III} (**3**), Ho^{III} (**4**), Y^{III} (**5**)) were obtained after two weeks.

The complexes are isostructural and crystallise in the triclinic space group $P\bar{1}$ (Table 1). The structure of **3** is described here as representative for the whole series, for which selected metrical parameters are summarised in Tables 1 and 2. The molecular structure (Figure 1) consists of a centrosymmetric $[Mn_5Dy_4]^{28+}$ core, held together by four $(\mu_3\text{-}O)^{2-}$ and two $(\mu_4\text{-}O)^{2-}$ ligands, and the oxygen atoms of two monodeprotonated $\eta^2{:}\eta^2{:}\eta^1{:}\mu_3$- and two doubly-deprotonated $\eta^3{:}\eta^2{:}\eta^1{:}\mu_4$-diethanolamine ligands. Peripheral ligation is provided by six μ-pivalate anions, four nitrate anions (one chelating each Dy ion) and a water molecule on each of Dy(2) and Dy(2a). The metal oxidation states (Mn^{III}, Mn^{IV}, Dy^{III}) and the deprotonation levels of O^{2-}, $mdea^{2-}$ and $mdeaH^-$ ions were established by charge considerations, bond valence sum calculations,[15] inspection of metric parameters and the observation of Jahn–Teller elongation axes of Mn^{III} (Table 2).

All five Mn atoms are six-coordinate. Dy(1) is nine-coordinate with a coordination polyhedron that may best be described as a triaugmented triangular prism, while Dy(2) is eight-coordinate and the coordination polyhedron could be described as between a distorted bicapped trigonal prism and a square antiprism. Inspection of the central core reveals two distorted $\{Mn^{IV}Mn^{III}Dy_2O_4\}$ cubanes sharing a Mn^{IV} vertex, Mn(1) (Figure 1). One oxo ligand in each cubane, O(1), bridges to a further Mn^{III} centre, Mn(3), which is further linked to Mn(2) and two Dy centres in the dicubane core by diethanolamine oxygen atoms. The monodeprotonated $mdeaH^-$ groups act as tridentate chelates on each of the outer Mn (Mn(3), Mn(3a)) atoms, while the two doubly-deprotonated $mdea^{2-}$ ions each chelate about a Dy centre, Dy(2). The Mn^{III} ions have the expected octahedral geometries with Jahn–Teller elongations along one axis,

Table 1. Crystallographic data for compounds **2–5**.

	2	**3**	**4**	**5**
formula	$C_{54}H_{110}Mn_5Tb_4N_{10}O_{40}$	$C_{54}H_{110}Mn_5Dy_4N_{10}O_{40}$	$C_{54}H_{110}Mn_5Ho_4N_{10}O_{40}$	$C_{54}H_{110}Mn_5Y_4N_{10}O_{40}$
M_r	2449.90	2464.22	2473.94	2169.86
crystal system	triclinic	triclinic	triclinic	triclinic
space group	$P\bar{1}$	$P\bar{1}$	$P\bar{1}$	$P\bar{1}$
a [Å]	13.7679(7)	13.7649(8)	13.7280(8)	13.7786(10)
b [Å]	13.9433(7)	13.9466(9)	13.9083(8)	13.9488(10)
c [Å]	14.0296(7)	14.0166(9)	13.9673(8)	14.0051(10)
α [°]	107.993(1)	108.045(1)	108.176(1)	108.215(1)
β [°]	109.831(1)	109.566(1)	109.302(1)	109.237(1)
γ [°]	109.096(1)	109.138(1)	109.150(1)	109.182(1)
V [Å^3]	2110.21(18)	2112.6(2)	2096.8(2)	2116.2(3)
Z	1	1	1	1
ρ_{calcd} [g cm^{-3}]	1.928	1.937	1.959	1.703
$\mu(Mo_{K\alpha})$ [mm^{-1}]	4.117	4.302	4.544	3.520
$F(000)$	1209	1213	1217	1127
T [K]	100	100	100	100
collected reflections	10824	10683	10583	10693
unique reflections	9097	9022	8940	8992
R_{int}	0.0164	0.0158	0.0169	0.0190
reflns with $I>2\sigma(I)$	7962	8039	7206	6691
refined parameters	521	521	521	521
R_1 [$I>2\sigma(I)$]	0.0247	0.0269	0.0284	0.0336
S (all data)	1.003	1.003	0.992	0.996
wR_2 (all data)	0.0573	0.0622	0.0555	0.0702

Table 2. Selected bond lengths and angles involving the bridging oxygen atoms for **2**, **3**, **4** and **5**, and calculated Mn valences.

2		**3**		**4**		**5**	
bond lengths							
Tb1–O2	2.317(2)	Dy1–O2	2.307(2)	Ho1–O5	2.296(3)	Y1–O5	2.304(2)
Tb1–O5	2.319(2)	Dy1–O5	2.307(2)	Ho1–O2	2.303(3)	Y1–O2	2.3056(19)
Tb1–O4	2.377(2)	Dy1–O4	2.371(2)	Ho1–O4	2.351(3)	Y1–O4	2.359(2)
Tb1–O1	2.485(2)	Dy1–O1	2.483(2)	Ho1–O1	2.465(3)	Y1–O1	2.476(2)
Tb1–O7	2.535(2)	Dy1–O7	2.526(2)	Ho1–O7	2.503(3)	Y1–O7	2.505(2)
Tb2–O4	2.319(2)	Dy2–O4	2.317(2)	Ho2–O4	2.299(3)	Y2–O4	2.300(2)
Tb2–O3	2.342(2)	Dy2–O3	2.334(2)	Ho2–O3	2.318(3)	Y2–O3	2.331(2)
Tb2–O1	2.407(2)	Dy2–O1	2.397(2)	Ho2–O1	2.378(3)	Y2–O1	2.382(2)
Mn1–O3	1.899(2)	Mn1–O3	1.898(2)	Mn1–O2	1.895(3)	Mn1–O3	1.8972(19)
Mn1–O2	1.8990(19)	Mn1–O2	1.900(2)	Mn1–O3	1.896(3)	Mn1–O2	1.9044(19)
Mn1–O1	1.9244(19)	Mn1–O1	1.926(2)	Mn1–O1	1.920(3)	Mn1–O1	1.9261(19)
Mn2–O2	1.884(2)	Mn2–O2	1.892(2)	Mn2–O2	1.885(3)	Mn2–O2	1.8862(19)
Mn2–O3	1.913(2)	Mn2–O3	1.915(2)	Mn2–O3	1.916(3)	Mn2–O3	1.917(2)
Mn2–O6′	2.169(2)	Mn2–O6′	2.173(2)	Mn2–O6′	2.165(3)	Mn2–O6′	2.172(2)
Mn2–O4	2.340(2)	Mn2–O4	2.345(2)	Mn2–O4	2.342(3)	Mn2–O4	2.354(2)
Mn3–O6	1.879(2)	Mn3–O6	1.880(2)	Mn3–O6	1.877(3)	Mn3–O6	1.882(2)
Mn3–O5	1.908(2)	Mn3–O5	1.913(2)	Mn3–O5	1.907(3)	Mn3–O5	1.911(2)
Mn3–O1	1.938(2)	Mn3–O1	1.939(2)	Mn3–O1	1.938(3)	Mn3–O1	1.9408(19)
Mn3–O7	2.331(2)	Mn3–O7	2.327(2)	Mn3–O7	2.317(3)	Mn3–O7	2.331(2)
bond angles							
Mn1-O1-Mn3	132.50(11)	Mn1-O1-Mn3	132.33(12)	Mn1-O1-Mn3	132.11(15)	Mn1-O1-Mn3	132.06(11)
Mn1-O1-Tb2	100.57(8)	Mn1-O1-Dy2	100.63(9)	Mn1-O1-Ho2	100.73(11)	Mn1-O1-Y2	100.83(8)
Mn3-O1-Tb2	120.70(9)	Mn3-O1-Dy2	121.01(10)	Mn3-O1-Ho2	120.89(12)	Mn3-O1-Y2	120.97(10)
Mn1-O1-Tb1	98.57(8)	Mn1-O1-Dy1	98.53(9)	Mn1-O1-Ho1	98.83(10)	Mn1-O1-Y1	98.65(8)
Mn3-O1-Tb1	92.32(8)	Mn3-O1-Dy1	92.17(8)	Mn3-O1-Ho1	92.27(10)	Mn3-O1-Y1	92.18(7)
Tb2-O1-Tb1	105.56(7)	Dy2-O1-Dy1	105.35(8)	Ho2-O1-Ho1	105.42(10)	Y2-O1-Y1	105.44(7)
Mn2-O2-Mn1	96.63(9)	Mn2-O2-Mn1	96.39(10)	Mn2-O2-Mn1	96.41(11)	Mn2-O2-Mn1	96.35(9)
Mn2-O2-Tb1	105.23(9)	Mn2-O2-Dy1	104.97(10)	Mn2-O2-Ho1	104.67(12)	Mn2-O2-Y1	104.84(9)
Mn1-O2-Tb1	105.37(9)	Mn1-O2-Dy1	105.65(9)	Mn1-O2-Ho1	105.46(11)	Mn1-O2-Y1	105.41(8)
Mn1-O3-Mn2	95.65(9)	Mn1-O3-Mn2	95.72(9)	Mn1-O3-Mn2	95.32(11)	Mn1-O3-Mn2	95.56(9)
Mn1-O3-Tb2	103.71(8)	Mn1-O3-Dy2	103.79(9)	Mn1-O3-Ho2	103.65(11)	Mn1-O3-Y2	103.55(8)
Mn2-O3-Tb2	105.57(9)	Mn2-O3-Dy2	105.44(10	Mn2-O3-Ho2	105.29(12)	Mn2-O3-Y2	105.30(9)
Tb2-O4-Mn2	93.67(7)	Dy2-O4-Mn2	93.30(8)	Ho2-O4-Mn2	93.30(10)	Y2-O4-Mn2	93.36(7)
Tb2-O4-Tb1	112.13(8)	Dy2-O4-Dy1	111.78(9)	Ho2-O4-Ho1	111.96(11)	Y2-O4-Y1	112.15(8)
Mn2-O4-Tb1	90.43(7)	Mn2-O4-Dy1	90.19(8)	Mn2-O4-Ho1	90.20(9)	Mn2-O4-Y1	89.98(7)
Mn3-O5-Tb1	98.47(8)	Mn3-O5-Dy1	98.51(9)	Mn3-O5-Ho1	98.57(12)	Mn3-O5-Y1	98.54(8)
Mn3-O6-Mn2′	125.13(10)	Mn3-O6-Mn2′	125.34(11)	Mn3-O6-Mn2′	125.59(13)	Mn3-O6-Mn2′	125.44(10)
Mn3-O7-Tb1	82.52(7)	Mn3-O7-Dy1	82.65(7)	Mn3-O7-Ho1	82.95(9)	Mn3-O7-Y1	82.88(7)
calculated Mn valences							
Mn1	3.92	Mn1	3.92	Mn1	3.96	Mn1	3.91
Mn2	2.89	Mn2	2.87	Mn2	2.89	Mn2	2.87
Mn3	2.86	Mn3	2.84	Mn3	2.87	Mn3	2.85

while the geometry of Mn^{IV} is a rather symmetric octahedron.

Magnetic properties: The dc magnetic susceptibility (χ) data for compounds **2**, **3**, **4** and **5** were collected in the 1.8–300 K temperature range at 1000 Oe as shown in Figure 2. For **3**, the room temperature χT value of 62.2 $cm^3 K mol^{-1}$ (Figure 2) is less than that expected (70.6 $cm^3 K mol^{-1}$) for four Mn^{III} ($S=2$), one Mn^{IV} ($S=3/2$) and four Dy^{III} ($S=5/2$, $L=5$, $^6H_{15/2}$) non-interacting ions. On the other hand, the static measurements for **2**, **4** and **5** lead to a room temperature χT value (67.8, 60.9 and 10.5 $cm^3 K mol^{-1}$) always in relatively good agreement with the values expected (61.1, 70.1 and 13.9 $cm^3 K mol^{-1}$) for isolated spin centres: four $S=2$ Mn^{III}, one $S=3/2$ Mn^{IV} and four Tb^{III} ($S=3$, $L=3$, $^7F_6$) in **2** or Ho^{III} ($S=2$, $L=6$, $^5I_8$) in **4** or Y^{III} ($S=0$) in **5** metal ions (Figure 2). On lowering the temperature, the χT product of **3** first gradually decreases to 50.2 $cm^3 K mol^{-1}$ around 17 K and then increases up to a value of 62.4 $cm^3 K mol^{-1}$ at 4.5 K, before it experiences a sharp drop to 54.4 $cm^3 K mol^{-1}$ at 1.8 K. Above 4.5 K, this behaviour is typically seen when antiferromagnetic (AF) interactions are dominant in a complex that possesses two types of spin that arrange in a ferrimagnetic manner. It should be noted that the thermal depopulation of the Dy^{III} excited states (Stark sublevels of the $^6H_{13/2}$ state) might also be partially responsible for the decrease of χT above 17 K. As shown in Figure 2, the temperature dependence of the dc susceptibility is similar for compounds **2** and **4** and thus the analysis of their experimental data is the same as for **3**. The non-compensation of the spin carriers suggests a large-spin ground state for these complexes. Moreover, the decrease of χT below 5 K is likely to be associated with intercomplex AF interactions and/or magnetic anisotropy.

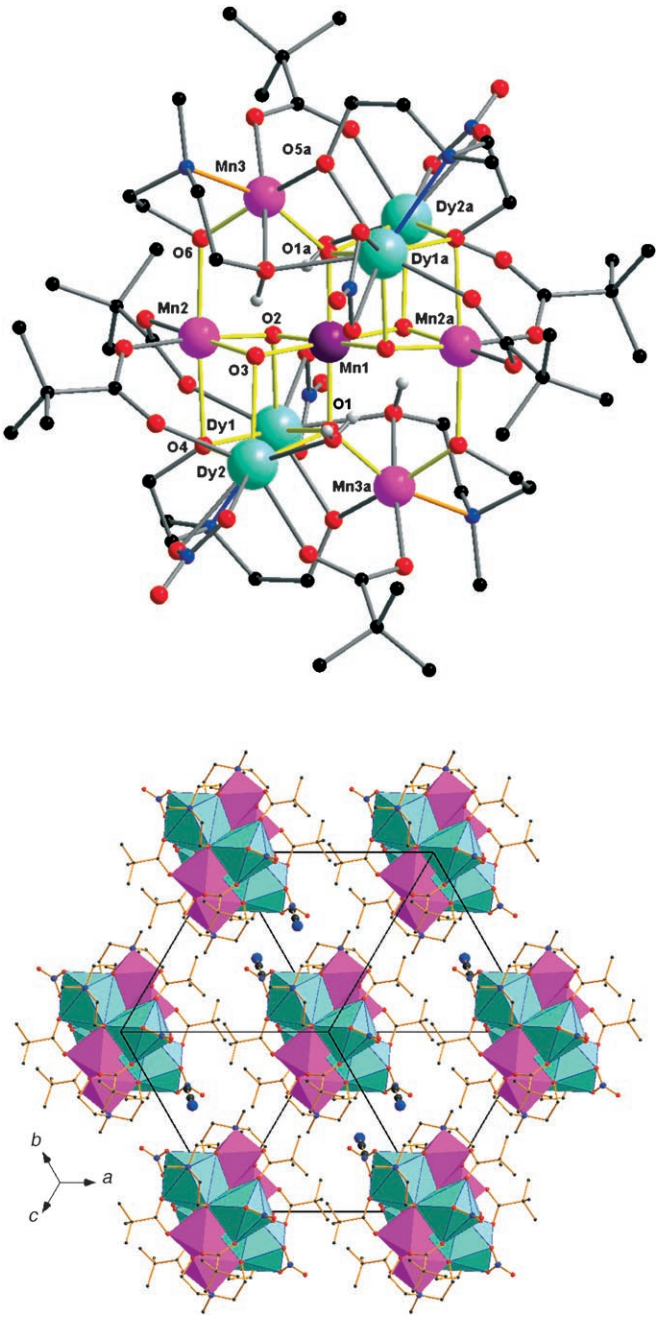

Figure 1. Molecular structure of **3** (top). Polyhedral view along the [1 1 1] direction (bottom). Organic H atoms are omitted for clarity. Dy green; Mn^{III} pink; Mn^{IV} purple; O red; N blue; C black, H white.

Field dependence of magnetisation (Figure S1, S3 and S6 in the Supporting Information) performed at 1.8 K for **2**, **3** and **4** reveals a lack of saturation even at 7 T indicating that 1) excited states are probably thermally and/or field-induced populated, but also 2) that magnetic anisotropy might be present, as expected for Mn^{III}- and Ln^{III}-based (with Ln^{III} = Tb^{III} and Dy^{III}) compounds.

In **5**, the Y^{III} ions are diamagnetic allowing us to independently study the magnetism of the $Mn^{III}_4Mn^{IV}$ unit. When the temperature is lowered at a field of 0.1 T, the χT product of **5** decreases to a minimum value of 1.8 $cm^3 K mol^{-1}$ at 1.8 K (Figure 2). Based on the structure of the compound, the χT product was simulated taking into account only three isotropic intracomplex magnetic interactions as shown in Scheme 1 and neglecting the low temperature data (below 20 K) to avoid additional effects coming from the magnetic anisotropy and/or weak intercomplex interactions. The following spin Heisenberg Hamiltonian [Eq. (1)] was thus considered in which J_1, J_2 and J_3 are the exchange interactions between Mn^{III} and Mn^{IV} sites through double O bridges between Mn^{III} and Mn^{IV} ions, through single O bridges, and between Mn^{III} ions through single alkoxo bridges, respectively, and S_i the spin vectors for each of the metal ions (S_i=2 for Mn^{III} with i=1–4 and S_5=3/2 for Mn^{IV}).

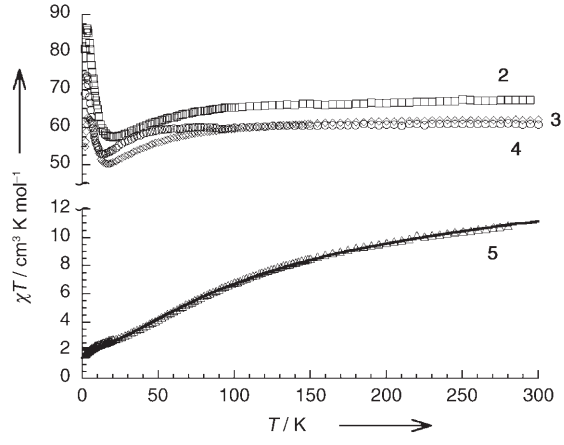

Figure 2. Temperature dependence of the χT product for polycrystalline samples of **2** (squares), **3** (rhombs), **4** (circles) and **5** (triangles) at 1000 Oe. The solid line that is superposed on the experimental data of **5** represents the best fit obtained with the model described in the text.

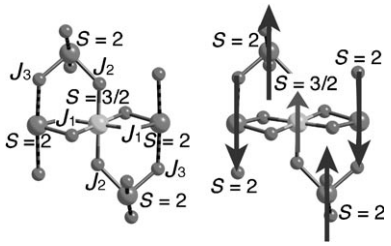

Scheme 1. Topology of the intra-complex magnetic interactions for **5**.

$$H = -2J_1S_5 \cdot (S_1 + S_3) - 2J_2S_5 \cdot (S_2 + S_4) - 2J_3(S_1 \cdot S_2 + S_3 \cdot S_4) \quad (1)$$

Using a numerical approach,[16] the simulation of the experimental data above 10 K gave $J_1/k_B = -45(2)$ K, $J_2/k_B = +6.0(5)$ K, $J_3/k_B = -9.0(5)$ K and $g = 2.1(1)$. Therefore even if ferromagnetic interactions are present between Mn^{III} and

Mn^{IV}, the AF interactions dominate and lead to a global decrease of the χT product at high temperature, as observed experimentally for all the reported compounds. This set of magnetic interactions induces an $S_T = 3/2$ ground state for **5** with the spin topology given in Scheme 1. At 1.85 K, M versus H measurements (Figure S7 in the Supporting Information) reveal a lack of a true saturation even at 7 T at which M reaches 2.7 μ_B in good agreement with an $S_T = 3/2$ ground state. The slow saturation of the magnetisation confirms also the presence of a significant anisotropy as expected in presence of Mn^{III} metal ions.

To probe the presence of slow dynamics in these molecular systems and thus the presence of SMM behaviour, ac susceptibility measurements were performed systematically on these compounds. The measurements were made in the 0.1–1500 Hz frequency range and at temperatures between 1.8 and 7 K. These four isostructural compounds display frequency-dependent out-of-phase signals (Figures 3 and 4, and Figures S4, S8 and S9 in the Supporting Information) suggesting that they behave as SMMs, but the properties are modulated by the metal ion used. The data as a function of the temperature or the ac frequency have been used together to determine the relaxation time (τ) for **2** and **3** and also their temperature dependence, which follows an Arrhenius law: $\tau = \tau_o \exp(\Delta_{eff}/k_B T)$ (Figure 3 bottom and Figure S5 in the Supporting Information). The values found for **2** and **3**, $\Delta_{eff} = 33/38.6$ K and $\tau_o = 4.5 \times 10^{-9}/3.0 \times 10^{-9}$ s, respectively, reveal that these complexes exhibit high-energy barriers with that for **3** being the highest recorded so far for 3d–4f SMMs.[11,12] The ac susceptibility measurements on **5**, performed in zero dc field, show the appearance of a very weak and noisy out-of-phase signal below 3 K exhibiting a significant frequency dependence. To reduce a possible fast zero-field relaxation induced by quantum tunnelling effects, a small dc field between 0 and 1 T was applied at 1.8 K (Figure S9 in the Supporting Information). The relaxation is dramatically slowed down from above 1500 Hz in zero field to 77 Hz in an optimum dc field of about 4500 Oe. To estimate the temperature dependence of the relaxation time, ac data were collected at 4500 Oe (Figure 4 right). Even if the two components of the ac susceptibility remain weak, as is to be expected for SMMs with small-spin ground state (here 3/2) and under a relatively large dc field, a clear maximum is now detected on the χ'' versus T data allowing an estimation of the energy gap at 20.2 K and τ_o as 2.6×10^{-8} s (Figure S10 in the Supporting Information).

Evidently the replacement of Y^{III} by Dy^{III} metal ions has an important effect on the SMM properties with an almost twofold enhancement of the energy gap from 20.2 to 38.6 K induced by an increase of the spin ground state and also most likely by an increase of the magnetic anisotropy. This latter hypothesis is supported by the magnetism of the Ho^{III} compound (**4**). The temperature dependence of the χT product (Figure 2) is similar to compound **3** reaching a maximum value of 73.4 $cm^3 K mol^{-1}$ at 3 K that suggests a large-spin ground state. Nevertheless, zero-field ac measurements for **4** are similar to those obtained for compound **5** with an ab-

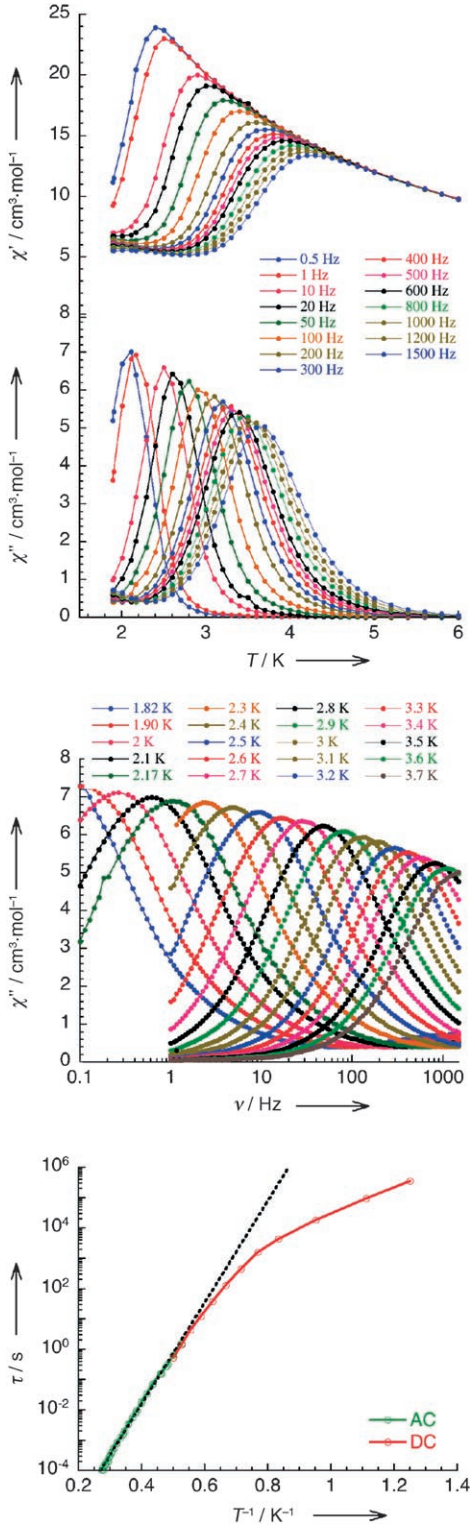

Figure 3. Temperature dependence of the in-phase (χ') and the out-of-phase (χ'') ac susceptibility components at different frequencies for **3** (top); out-of-phase *ac* susceptibility plots as a function of the frequency at different temperatures for **3** (centre); Arrhenius plot using ac (green) and dc (red) data. The dashed line is the fit of the thermally activated region (bottom).

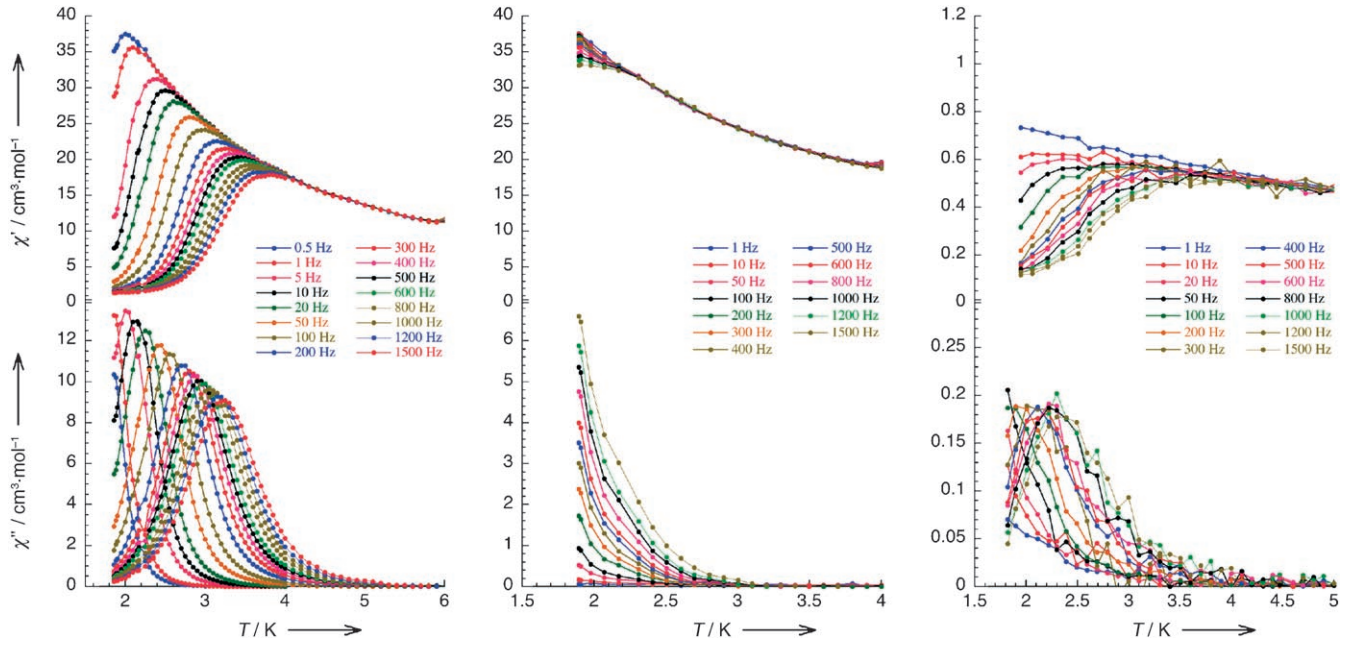

Figure 4. Temperature dependence of the in-phase (χ') and the out-of-phase (χ'') ac susceptibility component at different frequencies for **2** (left) and **4** (centre) in zero dc field and **5** in 4500 Oe (right).

sence of any χ'' maximum above 1.8 K even at 1500 Hz (Figure 4). In this case, like for **2** and **3** and unlike for **5**, even the application of small dc fields does not slow down the relaxation of the magnetisation, suggesting a weak influence of quantum effects in the temperature range studied. Thus, it is not possible to estimate a barrier height even if the similarity of the ac data between **4** and **5** suggests about the same energy gap (i.e., around 20 K). The replacement of the Y^{III} by Ho^{III} metal ions seems to have increased the spin ground state of the complex and modified its quantum properties, but unfortunately the energy gap remains roughly unchanged suggesting that the Ho^{III} contribution to the complex anisotropy is very weak.

The results from the Tb^{III} complex (**2**) further support the suggestion that the introduction of significant anisotropy is the key to providing larger energy barriers. Here the slow relaxation of the magnetisation detected in **2** (Figure 4 left) is very similar to that found for **3** (Figure 3) and clearly observed above 1.8 K. Below about 2 K, the relaxation time starts to deviate from the Arrhenius law suggesting the presence of quantum tunnelling of the magnetisation at lower temperatures (Figure 4 left and Figure S5 in the Supporting Information). We can conclude from these experimental results that in order to obtain large energy barriers and thus slow relaxation at the highest possible temperature it is important that through the introduction of the lanthanide ions not only the spin ground state but also the magnetic anisotropy is enhanced as observed in the case of the Dy^{III} analogue, **3**.

The slow relaxation of the magnetisation for **3** has also been studied by μ-SQUID measurements[17] on a single crystal. The field was aligned with a mean easy axis of magnetisation by using the transverse field method.[18] *M* versus *H* hysteresis loops were observed below 1.9 K at a field sweep rate of 0.002 $T s^{-1}$ (Figure 5 and Figure S2 in the Supporting Information). As expected for SMMs, the coercive field increases strongly with decreasing temperature and increasing scan rate, reaching about 1 T at 0.4 K. Below this temperature the *M* versus *H* data become temperature independent but remain strongly field sweep rate dependent, indicating that quantum tunnelling dominates the relaxation of the magnetisation. In Figure 5, a series of broad steps probably induced by resonant quantum tunnelling is also observed, but rather smeared out most likely by the presence of low-lying excited states and/or intercomplex interactions.[19,20]

Conclusion

In summary, we have presented a new family of high-nuclearity 3d–4f compounds, representing the first *N*-methyldiethanolamine-based Mn–Ln heterometallic complexes. All the present compounds show single-molecule magnet behaviour that is tuned by the choice of the lanthanide ion, with, in particular for compound **3**, the highest energy barrier reported to date for a heterometallic 3d–4f SMM. The series of molecular magnets reported in this paper highlight the importance of simple chemistry approaches in obtaining targeted series of pure molecular species showing interesting magnetic properties.

Experimental Section

Materials and methods: All the reactions were carried out under aerobic conditions. Unless otherwise stated all reagents were obtained from com-

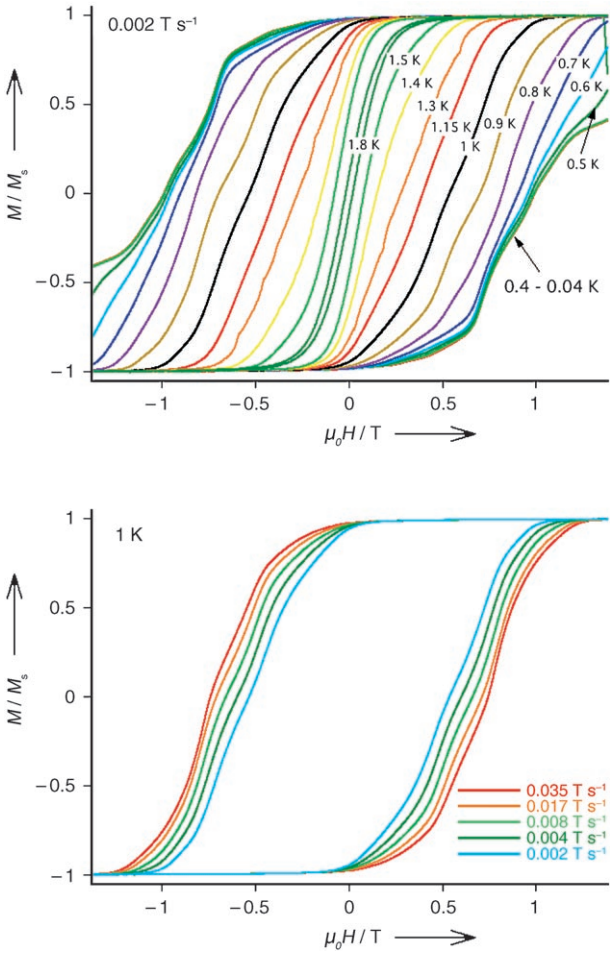

Figure 5. Field dependence of the magnetisation measured in the easy direction of a single crystal of **3**: (top) the temperature dependence at a fixed scan rate of 2 mT s^{-1}; (bottom) the scan-rate dependence at a fixed temperature of 1.0 K.

mercial sources, and were used as received, without further purification. All reactions were carried out under aerobic conditions. Elemental analyses for C, H and N were performed using an Elementar Vario EL analyser and were carried out at the Institute of Inorganic Chemistry, University of Karlsruhe. FTIR spectra were measured on a Perkin–Elmer Spectrum spectrometer with samples prepared as KBr discs.

$[Mn_6O_2(Piv)_{10}(4\text{-Me-py})_{2.5}(PivH)_{1.5}]$ (1): A slurry of $Mn(OAc)_2{\cdot}4H_2O$ (3.00 g, 12.00 mmol), $KMnO_4$ (1.90 g, 12.00 mmol) and pivalic acid (18.36 g, 180.00 mmol) was heated and maintained at reflux until the solution became colourless. The solution was cooled to 100 °C, then MeCN (10 mL) and 4-Me-py (0.6 mL) were added. The resulting mixture was again heated to boiling, then MeCN (30 mL) was added and the reaction mixture was cooled to room temperature. Red-brown crystals were formed after one day. They were recrystallised from 1:1 MeCN/CH_2Cl_2, filtered, washed with several portions of MeCN, and dried in air. Yield: 5.65 g (80.5 % based on Mn). Elemental analysis calcd (%) for $C_{72.5}H_{122.5}N_{2.5}O_{25}Mn_6$ (dried): C 49.51, H 7.02, N 1.99; found: C 49.71, H 7.19, N 1.82; IR (KBr): $\tilde{\nu}$ = 2960 (s), 2927 (m), 1692 (m), 1618 (m), 1591 (vs), 1570 (vs), 1482 (vs), 1458 (w), 1416 (vs), 1374 (s), 1359 (s), 1319 (w), 1229 (s), 1207 (m), 1030 (w), 1013 (w), 979 (w), 936 (w), 894 (w), 804 (w), 786 (w), 725 (w), 612 (s), 584 (m), 556 (m), 532 (w), 489 (w), 437 cm^{-1} (w).

Compound 3: $Dy(NO_3)_3{\cdot}6H_2O$ (0.30 g, 0.66 mmol) was added to a stirred slurry of **1** (0.20 g, 0.11 mmol) and *N*-methyldiethanolamine (0.147 g, 1.23 mmol) in MeCN (15 mL). After stirring for 5 min at room temperature, the mixture was heated under reflux for 40 min to give a dark-brown solution. The solution was allowed to cool, was filtered and was then left to evaporate slowly at room temperature. Brown crystals were obtained after two weeks, collected by filtration, washed with cold MeCN (5 mL), and dried in air. Yield: 70 mg (23.7 % based on Mn). Elemental analysis calcd (%) for $C_{50}H_{104}N_8O_{40}Mn_5Dy_4$ (dried): C 25.21, H 4.40, N 4.70; found: C 25.35, H 4.53, N 4.64; IR (KBr): $\tilde{\nu}$ = 3451 (m), 2961 (s), 2930 (s), 1591 (vs), 1568 (vs), 1485 (vs), 1416 (vs), 1374 (s), 1360 (s), 1295 (s), 1225 (s), 1081 (s), 1070 (s), 1029 (m), 999 (m), 937 (w), 816 (m), 787 (m), 758 (m), 742 (w), 700 (m), 621 (s), 533 (m), 510 (w), 421 cm^{-1} (w).

Compounds 2, 4 and 5: These compounds were obtained by the same procedure using $Tb(NO_3)_3{\cdot}6H_2O$, $Ho(NO_3)_3{\cdot}6H_2O$ and $Y(NO_3)_3{\cdot}6H_2O$ in place of $Dy(NO_3)_3{\cdot}6H_2O$. Their IR spectra are similar. Compound **2**: Yield: 0.06 g (18.9 % based on Mn); elemental analysis calcd (%) for $C_{50}H_{104}N_8O_{40}Mn_5Tb_4$ (dried): C 25.36, H 4.42, N 4.73; found: C 25.24, H 4.55, N 4.78. Compound **4**: Yield: 0.07 g (21.7 % based on Mn); elemental analysis calcd (%) for $C_{50}H_{104}N_8O_{40}Mn_5Ho_4$ (dried): C 25.11, H 4.38, N 4.68; found: C 25.21, H 4.44, N 4.58. Compound **5**: Yield: 0.05 g (17.7 % based on Mn); elemental analysis calcd (%) for $C_{50}H_{104}N_8O_{40}Mn_5Y_4$ (dried): C 28.76, H 5.02, N 5.36; found: C 28.59, H 4.94, N 5.44.

Physical measurements: X-ray data were collected at 100 K on a Bruker SMART Apex CCD diffractometers, and were corrected semiempirically[21a] for absorption. Structure solution by direct methods and full-matrix least-squares refinement against F^2 (all data) were carried out with the SHELXTL software package.[21b] CCDC 656728 (**2**), 656729 (**3**), 656730 (**4**), and 656731 (**5**) contains the supplementary crystallographic data for this paper. These data can be obtained free of charge from The Cambridge Crystallographic Data Centre via www.ccdc.cam.ac.uk/data_request/cif.

The magnetic susceptibility measurements were obtained with the use of a Quantum Design SQUID magnetometer MPMS-XL. This magnetometer works between 1.8 and 400 K for dc applied fields ranging from −7 to 7 T. Measurements were performed on finely ground polycrystalline samples. *M* versus *H* measurements were performed at 100 K to check for the presence of ferromagnetic impurities that were found to be systematically absent. The ac susceptibility measurements were measured with an oscillating ac field of 3 Oe and ac frequencies ranging from 0.1 to 1500 Hz. The magnetic data were corrected for the sample holder and the diamagnetic contributions.

Acknowledgements

This work was supported by the DFG (SPP 1137 and the Center for Functional Nanostructures), MAGMANet (NMP3-CT-2005-515767) and Bordeaux 1 University, the CNRS, the region Aquitaine and by the Alexander von Humboldt Foundation (V.M.).

[1] a) P. D. W. Boyd, Q. Li, J. B. Vincent, K. Folting, H.-R. Chang, W. E. Streib, J. C. Huffman, G. Christou, D. N. Hendrickson, *J. Am. Chem. Soc.* **1988**, *110*, 8537–8539; b) A. Caneschi, D. Gatteschi, R. Sessoli, *J. Am. Chem. Soc.* **1991**, *113*, 5873–5874; c) R. Sessoli, H.-L. Tsai, A. R. Schake, S. Wang, J. B. Vincent, K. Folting, D. Gatteschi, G. Christou, D. N. Hendrickson *J. Am. Chem. Soc.* **1993**, *115*, 1804–1816; d) R. Sessoli, D. Gatteschi, A. Caneschi, M. A. Novak, *Nature* **1993**, *365*, 141–143.

[2] T. Lis, *Acta Crystallogr. Sect. B* **1980**, *36*, 2042–2046.

[3] a) D. Gatteschi, R. Sessoli, *Angew. Chem.* **2003**, *115*, 278–309; *Angew. Chem. Int. Ed.* **2003**, *42*, 268–297; b) R. Bircher, G. Chaboussant, C. Dobe, H. U. Güdel, S. T. Ochsenbein, A. Sieber, O. Waldmann, *Adv. Funct. Mater.* **2006**, *16*, 209–220; c) O. Waldmann, *Inorg. Chem.* **2007**, *46*, 10035–10037.

[4] a) G. Christou, D. Gatteschi, D. N. Hendrickson, R. Sessoli, *MRS Bull.* **2000**, *25*, 66–71; b) J. P. Price, S. R. Batten, B. Moubaraki, K. S. Murray, *Chem. Commun.* **2002**, 762–763; c) E. C. Sanudo, W.

Wernsdorfer, K. A. Abboud, G. Christou, *Inorg. Chem.* **2004**, *43*, 4137–4144.
[5] D. N. Hendrickson, G. Christou, H. Ishimoto, J. Yoo, E. K. Brechin, A. Yamaguchi, E. M. Rumberger, S. M. J. Aubin, Z. Sun, G. Aromi, *Polyhedron* **2001**, *20*, 1479–1488.
[6] a) E. K. Brechin, M. Soler, G. Christou, J. Davidson, D. N. Hendrickson, S. Parsons, W. Wernsdorfer, *Polyhedron* **2003**, *22*, 1771–1775; b) E. K. Brechin, M. Soler, G. Christou, M. Helliwell, S. J. Teat, W. Wernsdorfer, *Chem. Commun.* **2003**, *11*, 1276–1277.
[7] a) H. Miyasaka, R. Clérac, W. Wernsdorfer, L. Lecren, C. Bonhomme, K. Sugiura, M. Yamashita, *Angew. Chem.* **2004**, *116*, 2861–2865; *Angew. Chem. Int. Ed.* **2004**, *43*, 2801–2805; b) H. Miyasaka, T. Nezu, K. Sugimoto, K. Sugiura, M. Yamashita, R. Clérac, *Chem. Eur. J.* **2005**, *11*, 717–724; c) L. Lecren, W. Wernsdorfer, Y.-G. Li, O. Roubeau, H. Miyasaka, R. Clérac, *J. Am. Chem. Soc.* **2005**, *127*, 11311–11317; d) C. Kachi-Terajima, H. Miyasaka, K.-i Sugiura, R. Clérac, H. Nojiri, *Inorg. Chem.* **2006**, *45*, 4381–4390; e) C. Kachi-Terajima, H. Miyasaka, A. Saitoh, N. Shirakawa, M. Yamashita, R. Clérac, *Inorg. Chem.* **2007**, *46*, 5861–5872.
[8] a) C. J. Milios, A. Vinslava, W. Wernsdorfer, S. Moggach, S. Parsons, S. P. Perlepes, G. Christou, E. K. Brechin, *J. Am. Chem. Soc.* **2007**, *129*, 2754–2755; b) C. J. Milios, A. Vinslava, W. Wernsdorfer, A. Prescimone, P. A. Wood, S. Parsons, S. P. Perlepes, G. Christou, E. K. Brechin, *J. Am. Chem. Soc.* **2007**, *129*, 6547–6561.
[9] a) F. Mori, T. Ishida, T. Nogani, *Polyhedron* **2005**, *24*, 2588–2592; b) M. Murugesu, A. Mishra, W. Wernsdorfer, K. A. Abboud G. Christou, *Polyhedron* **2006**, *25*, 613–625; c) M. Ferbinteanu, T. Kajiwara, K.-Y. Choi, H. Nojiri, A. Nakamoto, N. Kojima, F. Cimpoesu, Y. Fujimura, S. Takaishi, M. Yamashita, *J. Am. Chem. Soc.* **2006**, *128*, 9008–9009; d) J.-P. Costes, J.-M. Clemente-Juan, F. Dahan, J. Milon, *Inorg. Chem.* **2004**, *43*, 8200–8202; e) J.-P. Costes, F. Dahan, W. Wernsdorfer, *Inorg. Chem.* **2006**, *45*, 5–7.
[10] a) F. Mori, T. Nyui, T. Ishida, T. Nogami, K-Y. Choi, H. Nojiri, *J. Am. Chem. Soc.* **2006**, *128*, 1440–1441; b) S. Osa, T. Kido, N. Matsumoto, N. Re, A. Pochaba, J. Mrozinski, *J. Am. Chem. Soc.* **2004**, *126*, 420–421.
[11] a) C. Aronica, G. Pilet, G. Chastanet, W. Wernsdorfer, J.-F. Jacquot, D. Luneau, *Angew. Chem.* **2006**, *118*, 4775–4778; *Angew. Chem. Int. Ed.* **2006**, *45*, 4659–4662; b) V. Chandrasekhar, B. M. Pandian, R. Azhakar, J. J. Vittal, R. Clérac, *Inorg. Chem.* **2007**, *46*, 5140–5142.
[12] M. Mereacre, A. M. Ako, R. Clérac, W. Wernsdorfer, G. Filoti, J. Bartolomé, C. E. Anson, A. K. Powell, *J. Am. Chem. Soc.* **2007**, *129*, 9248–9249.
[13] A. M. Ako, V. Mereacre, I. J. Hewitt, R. Clérac, L. Lecren, C. E. Anson, A. K. Powell, *J. Mater. Chem.* **2006**, *16*, 2579–2586.
[14] a) A. Mishra, W. Wernsdorfer, K. A. Abboud, G. Christou, *J. Am. Chem. Soc.* **2004**, *126*, 15648–15649; b) C. Zaleski, E. Depperman, J. Kampf, M. Kirk, V. Pecoraro, *Angew. Chem.* **2004**, *116*, 4002–4004; *Angew. Chem. Int. Ed.* **2004**, *43*, 3912–3914; c) A. Mishra, W. Wernsdorfer, S. Parson, G. Christou, E. Brechin, *Chem. Commun.* **2005**, 2086–2088.
[15] W. Liu, H. H. Thorp, *Inorg. Chem.* **1993**, *32*, 4102–4105.
[16] a) J. J. Borrás-Almenar, J. M. Clemente-Juan, E. Coronado, B. S. Tsukerblat, *Inorg. Chem.* **1999**, *38* , 6081–6088; b) J. J. Borrás-Almenar, J. M. Clemente-Juan, E. Coronado, B. S. Tsukerblat, *J. Comput. Chem.* **2001**, *22*, 985–991.
[17] W. Wernsdorfer, *Adv. Chem. Phys.* **2001**, *118*, 99–190.
[18] W. Wernsdorfer, N. E. Chakov, G. Christou, *Phys. Rev. B* **2004**, *70*, 132413/1–132413/4.
[19] D. Foguet-Albiol, T. A. O'Brien, W. Wernsdorfer, B. Moulton, M. Zaworotko, K. A. Abboud, G. Christou, *Angew. Chem.* **2005**, *117*, 919–923; *Angew. Chem. Int. Ed.* **2005**, *44*, 897–901.
[20] a) A. M. Ako, I. J. Hewitt, V. Mereacre, R. Clérac, W. Wernsdorfer, C. E. Anson, A. K. Powell, *Angew. Chem.* **2006**, *118*, 5048–5051; *Angew. Chem. Int. Ed.* **2006**, *45*, 4926–4929; b) A. J. Tasiopoulos, A. Vinslava, W. Wernsdorfer, K. A. Abboud, G. Christou *Angew. Chem.* **2004**, *116, 2169–2173; Angew. Chem. Int. Ed.* **2004**, 43, 2117–2121; *Angew. Chem. Int. Ed.* **2004**, *43*, 2117–2121; c) H. Miyasaka, K. Nakata, L. Lecren, C. Coulon, Y. Nakazawa, T. Fujisaki, K. Sugiura, M. Yamashita, R. Clérac, *J. Am. Chem. Soc.* **2006**, *128*, 3770–3783.
[21] a) G. M.Sheldrick, SADABS (the Siemens Area Detector Absorption Correction), University of Göttingen, **1996**; b) G. M. Sheldrick, SHELXTL 6.14, Bruker AXS Inc., 6300 Enterprise Lane, Madison, WI 53719–1173, USA, **2003**.

Received: January 22, 2008
Published online: March 17, 2008

